



Effects of Re on microstructure evolution of nickel-based single crystal superalloys

Zhongkui Zhang^{1,2} · Zhixun Wen¹ · Zhufeng Yue¹

Received: 29 March 2020 / Accepted: 28 July 2020 / Published online: 7 August 2020
© Springer-Verlag GmbH Germany, part of Springer Nature 2020

Abstract

The high temperature creep and long-term aging tests of the second-generation (DD6) and the third-generation (DD9) single crystal superalloys with different Re contents were carried out. The effects of Re, dislocations, TCP phases and their interaction on creep properties and microstructure evolution were researched. The third-generation single crystal superalloy has the more compact and uniform two-phase structure and the better creep properties. The rafting rate in dendrite is higher than that in interdendrite. The γ' phases connect into a stripline, the γ phases on the strip line are truncated, and the TCP phase is precipitated along the stripline. The element Re carries out the pipe diffusion and the vacancy diffusion at the high temperature. The TCP phase precipitates in the region with many dislocations and vacancies. Re hinders the movement of dislocations and promote the precipitation of TCP phases. The movement of dislocations promotes the diffusion of Re and the precipitation of TCP phases. TCP phases promote the diffusion of elements and accelerate the rafting of γ' phases.

Keywords Re · Rafting · TCP phase · Dislocation · Single crystal

1 Introduction

Nickel-based single crystal superalloys have been widely used in the hot part of the aero-engine because of their excellent high temperature creep resistance and oxidation resistance [1–4]. At present, almost all aero-engines use nickel-based single crystal superalloys as the blade materials, and the nickel-based single crystal superalloys have developed to the fifth generation (TMS-162). For every 55° increase in the temperature bearing capacity of the turbine blade of the aero-engine, the efficiency can be increased by 10% [5]. At present, the aero-engine turbine blade materials in service are mostly the second-generation and the third-generation single crystal superalloys, and the temperature bearing capacity of each generation is about 30° higher than that of the previous [2, 6]. Conducting researches on high-temperature properties and basic theory of nickel-based single

crystal superalloys to accelerate the upgrading of single-crystal materials has great significance to the development of the aviation industry.

In the development of single crystal superalloys, the refractory element Re has the greatest effect on improving the mechanical properties [7]. 3% Re and 6% Re are almost the main features and differences of the second-generation and the third-generation single crystal superalloys. The addition of Re can significantly improve the temperature bearing capacity of single crystal superalloys [8–11]. Taking a typical two-generation single crystal in the United States as an example, the third-generation single-crystal CMSX-10 (6% Re) has the advantage of 36 °C and 25 °C temperature bearing capacity over the second-generation single-crystal CMSX-4 (3% Re) with 1% creep strength at 207 MPa and 138 MPa, respectively [12]. However Re is a strategic scarce element, and the addition of 1% Re doubles the casting cost of single crystal superalloys. Micropores are also prone to appear in the directional solidification and solid solution treatment [13]. It has great theoretical and engineering significance to find out the strengthening mechanism and alternative element of Re to reduce the casting cost. Y. Ru et al. [14] tried to replace Re with Mo in single crystal superalloys but still lacked engineering application verification. In view of this, some scholars have studied the strengthening mechanism of Re on single crystal superalloys.

✉ Zhongkui Zhang
zkzhang@mail.nwpu.edu.cn

¹ School of Mechanics, Civil Engineering and Architecture, Northwestern Polytechnical University, Xi'an 710072, People's Republic of China

² Xi'an University of Posts and Telecommunications, Xi'an 710121, People's Republic of China

P. Wollgramm et al. [15] believed that the strengthening mechanism of Re was due to the short-range order Re clusters in the γ phase. However, A. Mottura et al. [16] had an opposite conclusion, that Re clusters did not exist in the γ phase, and weren't the reason for the strengthening of Re on single crystal superalloys. Re can promote the reverse distribution of other elements in the γ phase and γ' phase, reduce the distribution proportion of part elements in the γ' phase and inhibit the growth of the γ' phase [17, 18]. The large volume fraction of γ' phases causes the supersaturation of Re in γ phases [19]. But the strengthening mechanism of the interaction between Re and γ' phases is still unclear. The addition of Re promotes the formation of dense dislocation networks at the γ/γ' phase interface, block the dislocation from cutting into the γ' phase, reduce the lattice misfit of γ/γ' phases, lower the rafting rate of γ' phases, and improve the creep properties of single crystal superalloys [18, 20]. The lattice misfit has an important effect on the rafting direction and rafting rate of γ' phases [21]. R. C. Reed et al. [2, 22, 23] believed that Re improved the properties of single crystal superalloys by solution hardening. K. Chen et al. [24, 25] considered that Re enhanced the temperature bearing capacity and creep resistance of single-crystal superalloys by strengthening the γ/γ' phase interface. S. Y. Ma et al. [26] thought that the blocking effect of Re on dislocations was stronger than that of W and Cr, and Re had a stronger alloying effect in single crystal superalloys. At present, there is still no unified understanding of the strengthening mechanism of Re on the performance of single crystal superalloys.

Re is mainly segregated in dendrite [27]. The increase of Re content increases the density of alloys and reduces the working efficiency of the engine. At the same time, TCP phases precipitate during the high-temperature long-term aging or endurance tests in the dendrite [28], and the spatial arrangement and the shape of the TCP phase are influenced by the stress/strain [29]. The precipitation of TCP phases consumes a large amount of refractory elements [30, 31], blocks the rafting γ' phase, and then seriously weaken the strengthening effect of Re on single crystal superalloys. So far, there is still no complete and unified understanding of the formation mechanism of TCP phases and the segregation mechanism of Re in TCP phases.

In this paper, the high temperature creep and long-term aging experiments of the second-generation and the third-generation single crystal superalloys with different Re contents were carried out. The effects of Re, dislocations, and TCP phases and their interaction on creep properties and microstructure evolution were researched.

2 Experiments

The materials considered here are the second-generation and the third-generation single crystal superalloys with different Re contents. The chemical compositions are listed in Table 1. All test samples were prepared from the [001] oriented bar which was cast in a directional solidification vacuum furnace under a high thermal gradient. The crystal orientation was examined by X-ray Laue back diffraction. The heat treatment regime of DD6 is given as follows: 1290 °C, 1 h + 1300 °C, 2 h + 1315 °C, 4 h, air cooling (AC) + 1120 °C, 4 h, AC + 870 °C, 32 h, AC. The heat treatment regime of DD9 is given as follows: 1340 °C, 6 h, AC + 1120 °C, 4 h, AC + 870 °C, 32 h, AC. The geometrical details of the creep specimen are shown in Fig. 1 along with the major dimension. The specimen for the long-term aging test is a cube of 7 × 5 × 3 mm, in which 7 mm × 5 mm is the [001] plane.

The creep tests were performed on a CSS-RDL 100 creep testing machine. The loading rate was 1 kN/min, and the loading direction was in line with the [001] axis. The uniaxial constant load creep tests along the [001] direction were conducted in air at 1100 °C and 140 MPa. The temperature was monitored using a thermocouple with an error of ± 3 °C. The temperature approached the target value

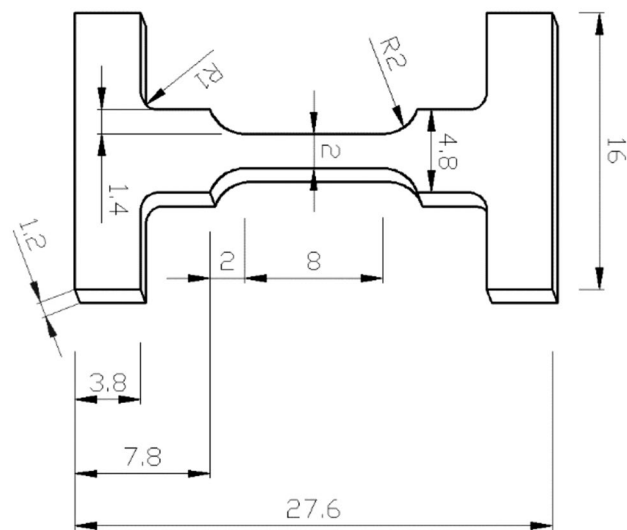


Fig. 1 Geometry of creep test specimen (mm)

Table 1 Chemical composition of nickel-based single crystal superalloys / Mass%

Alloy	C	Cr	Co	W	Mo	Al	Ta	Nb	Re	Hf	Ni
DD6	0.001–0.04	3.8–4.8	8.5–9.05	7.0–9.0	1.5–2.5	5.2–6.2	6.0–8.5	0–1.2	1.6–2.4	0.05–1.5	Balance
DD9	0.0–0.04	1.5–5.0	5.5–9.5	6.0–8.5	0.5–3.0	5.2–6.2	5.5–9.0	0.0–1.5	3.5–5.0	0.0–0.5	Balance

and was maintained for 0.5 h before the experiment. After the creep test, the sample was cut, mechanically ground, polished and chemically corroded using 5 ml nitric acid, 10 ml hydrofluoric acid and 15 ml hydrogen peroxide for the scanning electron microscopy (SEM) analysis. The SEM investigation was performed using a JSM-6390 working at 30 kV with energy-dispersive X-ray spectroscopy (EDS). The spot size was 40 μm . The size and volume fraction of the γ phase and the γ' phase were measured by the software Image J after a binary processing, taking the average value for ten measurements. An FEI Talos F200X field-emission transmission electron microscope (TEM) was used to study the morphology of dislocations after the creep. To avoid the influence of necking on the dislocation, we cut the sample for TEM at a position approximate 3 mm from the necked region. After mechanically grinding below 50 μm , TEM foils were double spray electrolytic thinning in a solution of 10 ml perchloric acid and 90 ml ethanol at $-40\text{ }^\circ\text{C}$ and -30 mA . The TEM bright field (BF) photos of dislocations are taken with the operation vector $\mathbf{g} = \langle 020 \rangle$ and the zone axis $\mathbf{B} = [001]$.

3 Results

3.1 Creep properties

The creep curves of DD6 and DD9 at 1100 $^\circ\text{C}$ and 140 MPa are shown in Fig. 2. Compared to DD6, DD9 has a longer creep life and the larger strain at the same temperature and stress. The initial creep stage of DD6 is relatively short, and the steady creep stage starts after 0.93 h. This means the steady creep stage starts almost after the elastic deformation, and the creep strain is 2.18%. The initial creep stage curve of DD9 is similar to that of DD6. The steady creep stage of DD9 starts after 1.1 h, and the creep strain is 1.91%. The creep time and strain in the initial creep stage of DD6 and

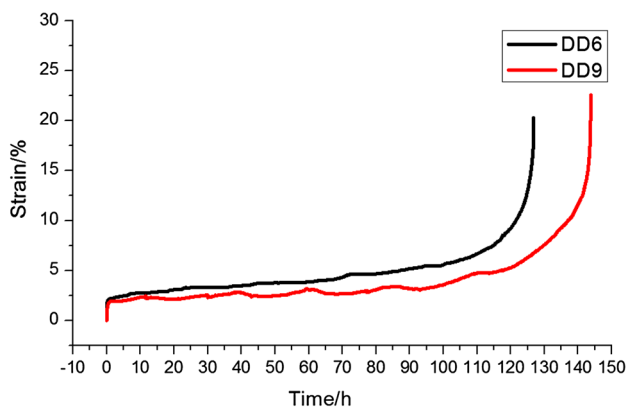


Fig. 2 The creep curves of DD6 and DD9

DD9 are similar. The creep strain of DD6 and DD9 increases at a constant rate in the steady creep stage. The tertiary creep stage of DD6 starts after the steady creep 98.42 h, and the creep strain is 3.33%. The tertiary creep stage of DD9 starts after the steady creep 114.43 h, and the creep strain is 2.93%. In the steady creep stage, the creep time of DD9 is greater than DD6, and the creep strain is less than DD6. In the tertiary stage, the creep time of DD6 and DD9 is 27.44 h and 28.24 h, and the creep strain is 14.78% and 17.76%, respectively. The creep life and creep strain of DD6 are less than that of DD9.

3.2 Microstructure

The morphologies of DD6 and DD9 before and after the creep tests are shown in Fig. 3. Compared Fig. 3a, b, it can be seen that DD6 and DD9 with different Re contents have different microstructures. The size and distribution of γ phases and the cubic γ' phases in DD9 are more uniform, but the size of a single γ' phase in DD6 is larger. Before the creep test of DD6, the width of the γ phase and the γ' phase are 0.1243 μm and 0.4375 μm , respectively, and the volume fraction of γ' phases is 66.55%, as shown in Fig. 3a. Before the creep test of DD9, the width of the γ phase and the γ' phase are 0.1186 μm and 0.3628 μm , respectively, and the volume fraction of γ' phases is 65.32%, as shown in Fig. 3b. After the creep test, it can be seen from Fig. 3c, d that the γ' phases in DD6 and DD9 raft completely, and the rafting dissolves is occurred in the DD6. The width of the γ phase and the γ' phase of DD6 are 0.6651 μm and 1.8062 μm , and the width of the γ phase and the γ' phase of DD9 are 0.48 μm and 1.0987 μm , respectively, as shown in Fig. 3c, d. The changes in the width of the γ phase and the γ' phase of DD6 are 0.5408 μm and 1.3687 μm . The changes in the width of the γ phase and the γ' phase of DD9 are 0.3614 μm and 0.7359 μm . The widths of the γ phase and the rafting γ' phase of DD6 are larger than that of DD9, and the change of size difference is consistent with the above. The rafting and rafting dissolution of DD6 are thoroughly. The γ phase and the rafting γ' phase of DD9 are more ordered.

3.3 Morphologies of TCP phases and γ/γ' phases

The morphologies of TCP phases of DD6 and DD9 are shown in Fig. 4. Compared Fig. 4a, b, there are great differences in the growth direction and the number of TCP phases between DD6 and DD9 after the creep tests.

The morphologies of DD9 with different aging times are shown in Fig. 5. The γ' phase is still cubic with aging for 10 h, as shown in Fig. 5a. Compared to Fig. 3b, it can be seen from Fig. 5a that the cubic γ' phase changes slightly, and no TCP phase is precipitated. Some regions connect into a strip, as shown in the red rectangles in Fig. 5a. After aging

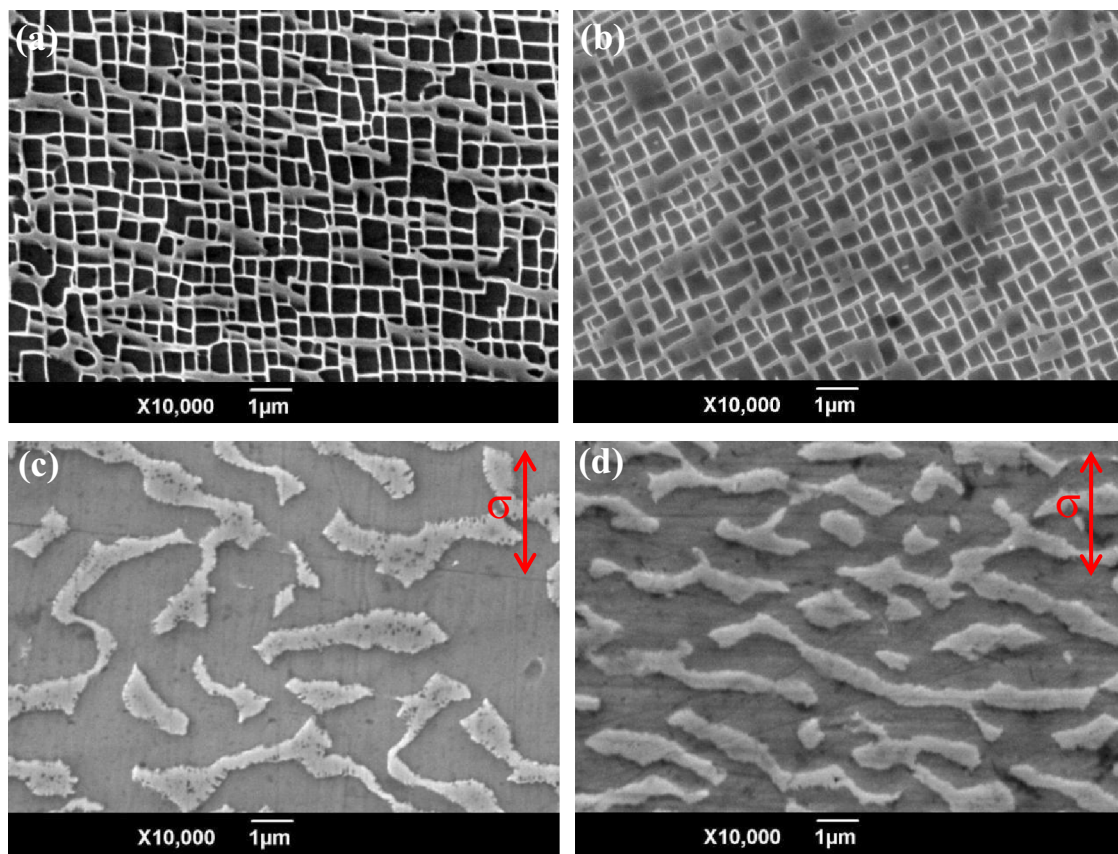


Fig. 3 The morphologies of DD6 and DD9: (a) 0 h (DD6), (b) 0 h (DD9), (c) failure (DD6), (d) failure (DD9)

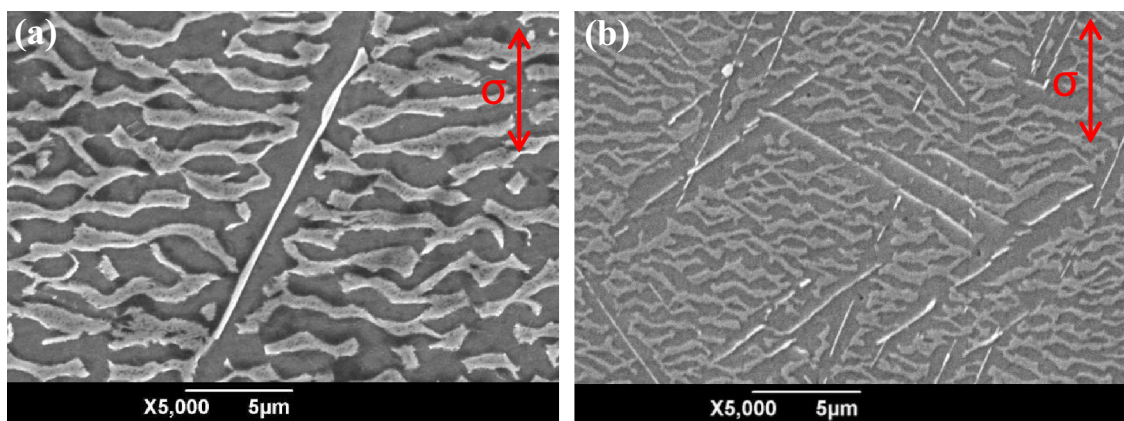


Fig. 4 The morphologies of TCP phases of DD6 and DD9: (a) DD6, (b) DD9

for 15 h, many TCP phases are formed, and the γ' phases are still approximately cubic except the region near the TCP phase, as shown in Fig. 5b. After aging for 40 h, the number of TCP phases increase, and the γ' phases are still cubic, as shown in Fig. 5c. After aging for 80 h, some of the γ' phases have already began to raft, and the γ' phases far from the TCP phase are still cubic, as shown in Fig. 5d. From

Fig. 5a–d, it can be seen that the γ' phases are approximately cubic except the region near the TCP phase. The shape of the γ' phase near the TCP phase has a big change.

After aging for 100 h, the γ' phases distribute uneven and cannot remain intact cubic. A small amount of γ' phases connect to each other, the rafting quickening and the γ phase coarsening, as shown in Fig. 5e. After aging for 150 h, part

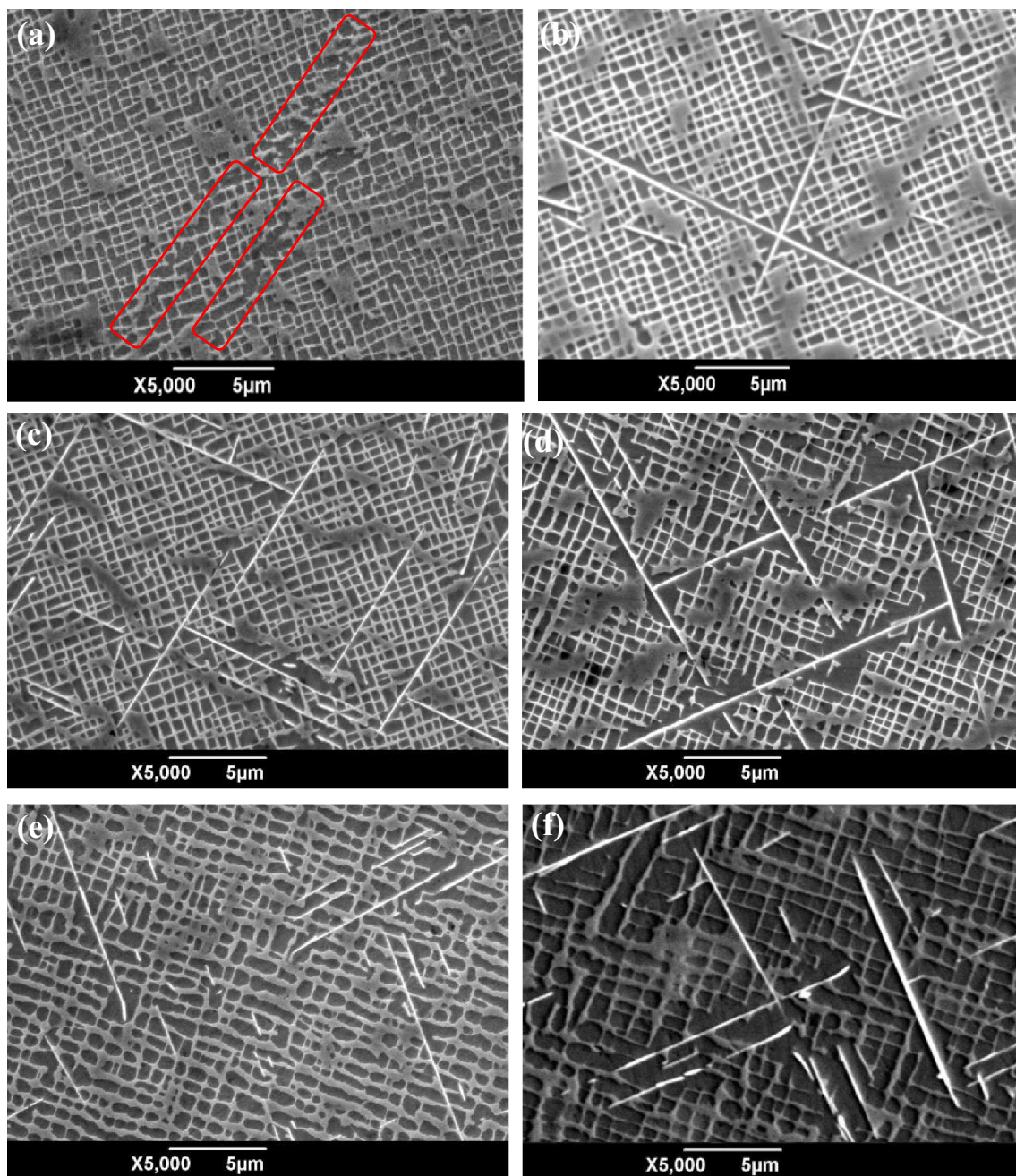


Fig. 5 The morphologies of DD9 at different aging times: (a) 10 h, (b) 15 h, (c) 40 h, (d) 80 h, (e) 100 h, (f) 150 h, (g) 200 h, (h) 400 h, (i) 600 h, (j) 800 h

of the γ phases are consumed and the rafting of γ' phases is further, as shown in Fig. 5f. During the long-term aging for 80–150 h, the cubic γ' phases gradually disappear and the whole rafting begins. Compared Fig. 3d and Fig. 5f, it can be seen that the rafting rate of creep test is higher than that of the long-term aging test at a similar test time. The applied stress can quicken the rafting.

After aging for 200 h, the two-phase structure is destroyed, a larger number of TCP phases are formed, many

γ phases are consumed, and a large number of γ' phases connect into one, as shown in Fig. 5g. After aging for 400 h, the two-phase structure is destroyed completely, and no cubic γ' phase is found, as shown in Fig. 5h. After aging for 600 h, the rafting of γ' phases has been basically completed, as shown in Fig. 5i. After aging for 800 h, many γ phases connect into a sheet, as shown in Fig. 5j. Compared to Fig. 3d, the rafting of the long-term aging test is more chaotic. The comparative analysis on Fig. 5b–j shows that TCP phases

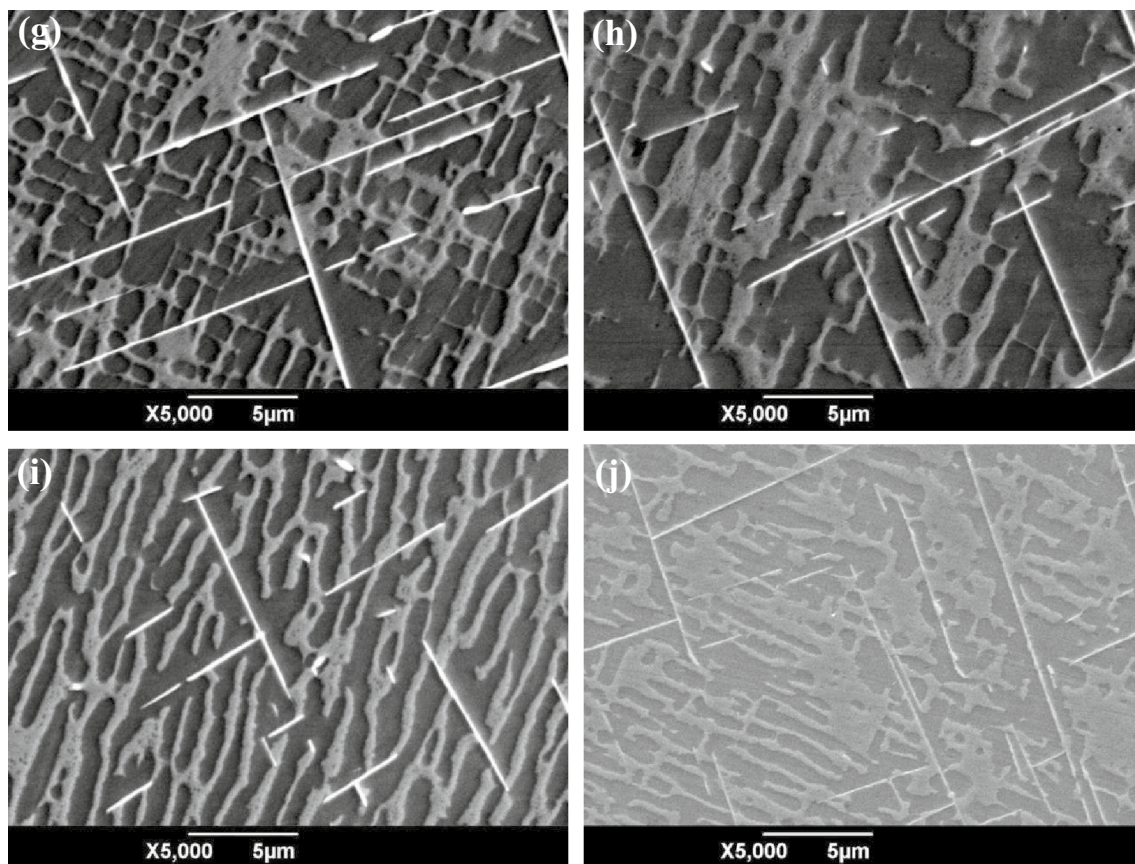


Fig. 5 (continued)

have been precipitated in the early stage and grow along with two approximately perpendicular directions at different aging times.

Figure 6 shows the interdendritic morphologies of DD9 with different aging times. After aging for 80 h, only a small amount of γ' phases connect to each other in the

interdendrite, as shown in the red rectangles of Fig. 6a. After aging for 800 h, the γ/γ' two-phase structure is still obvious, as shown in Fig. 6b, which is similar to the dendritic morphology after aging for 100 h in Fig. 5e, indicating that there is a great difference in the micromorphology between the dendrite and the interdendrite. No TCP phase is precipitated

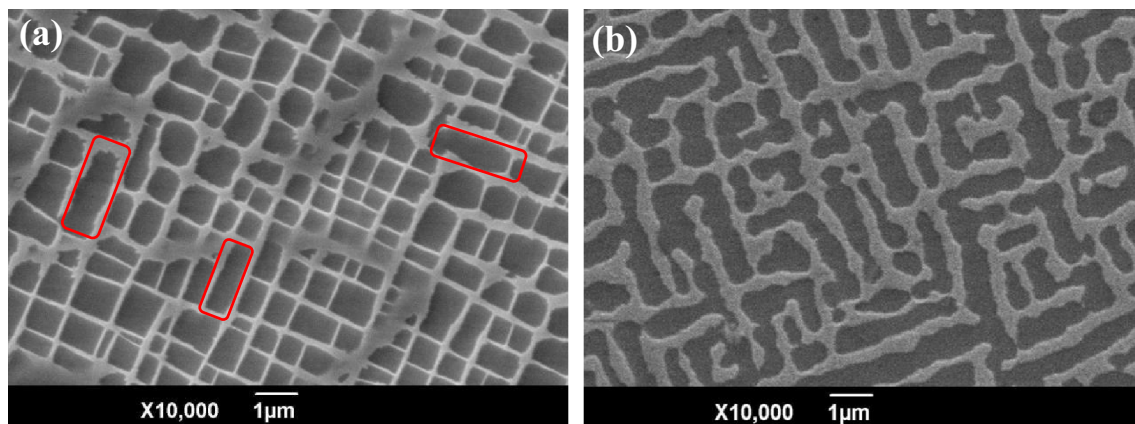


Fig. 6 The morphologies of DD9 at different aging times in the interdendrite: (a) 80 h, (b) 800 h

in the interdendrite. From 80–800 h, it can be seen that the microstructure in interdendrite evolves slowly.

The EDS spots of DD9 before the test are given in Fig. 7. The average content of Re in percentage for three measurements with a low dispersion is given in Table. 2.

From Table 2 it can be seen that Re mainly segregates in the dendrite. The Re content of γ phase in the dendrite is 31.28% higher than that of γ phase in the interdendrite. The Re content in the γ' phase is close to zero.

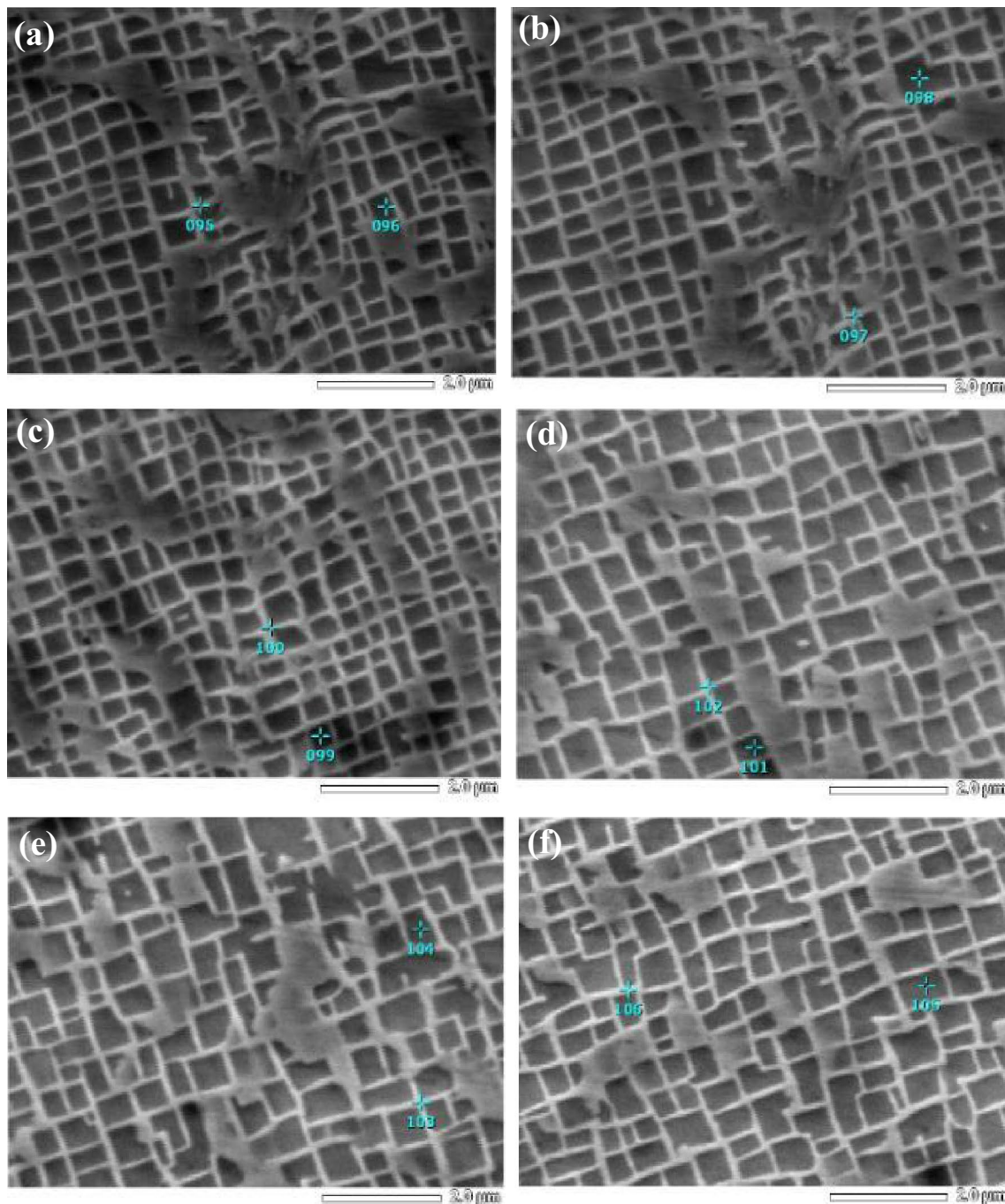


Fig. 7 The EDS spot in dendrite/interdendrite: (a–c) dendrite, (d–f) interdendrite

Table 2 The Re content of γ/γ' phases in dendrite/interdendrite mass%

Region	Phase	Spot 1		Spot 2		Spot 3		Average	
		Re	Error	Re	Error	Re	Error	Re	Error
Dendrite	γ	4.99	0.23	4.46	0.27	4.66	0.24	4.70	0.25
	γ'	0.21	0.28	0.40	0.29	0	0	0.20	0.19
Interdendrite	γ	3.68	0.26	4.01	0.21	3.06	0.28	3.58	0.25
	γ'	0.53	0.30	0	0	0	0	0.18	0.10

4 Discussions

4.1 The effect of Re on creep properties

At the same temperature and stress, DD9 has the longer creep life and creep strain than that of DD6, indicating that DD9 has the better creep property at 1100 °C and 140 Mpa. This is related to the content of Re, and the evolution of the microstructure occurs diffusion controlled [32]. In the initial creep stage, the creep curves of DD6 and DD9 are similar, which indicates that DD6 and DD9 have a similar elastic property. We think this is related to the same two-phase microstructure and the similar element composition. It can be deduced that the effect of Re on the elastic property of DD6 and DD9 is slight. The addition of Re increases the diffusion activation energy of other elements. The study [17] shows that the diffusion activation energy of Al increased from 2.072 eV to 3.438 eV after adding the element Re. The increase of diffusion activation energy means the increase of binding energy between atoms. Therefore, DD9 containing more Re has greater creep time and smaller creep strain in the steady creep stage. A large number of TCP phases are precipitated in the steady creep stage, which consumes the element Re, seriously reduce the plasticity of the single crystal superalloy and the hindrance on dislocations [33, 34]. Therefore, the creep strain increases rapidly in the tertiary stage. Due to the more precipitation of TCP phases, the creep strain of DD9 (17.76%) in the tertiary creep stage is greater than that of DD6 (14.78%).

4.2 The strengthening effect of Re on microstructure

In the section 3.2, we know that the microstructure (size, volume fraction and size difference of γ and γ' phase) are different. High levels of Re can reduce the size of γ phase and γ' phase, and make the distribution of γ phases and γ' phases more uniform. At the same time, the finer and more uniform γ' increases the γ/γ' phase interfacial area, improves the hindrance of the γ/γ' interface to the motion of dislocations, and then enhances the interfacial strengthening effect. The initial fine and uniform γ' phase of DD9 makes the rafting more orderly, and the distribution of γ phases and γ' phases is more uniform after the rafting. The low diffusion

rate of Re reduces the rafting rate of γ' phases. After the creep, the changes of the γ phase and the γ' phase of DD6 are greater than that of DD9, which are corresponding to the changes of creep strain. The microstructure of DD9 is more stable than that of DD6.

Compared Fig. 3d and Fig. 5f, the rafting is more thoroughly and the evolution of microstructure is more drastic in the creep test than that of the long-term aging test. This is because stress can provide higher migration energy and promote the directional migration of elements. Therefore, the applied stress can promote the rafting of γ' phases. In the long-term aging test, an obvious result of the directional migration of Re is the precipitation of TCP phases in the dendrite due to the higher Re content. The precipitation of TCP phase consumes Re in the dendrite, seriously weakens the strengthening effect of Re on the microstructure, enhances the overall diffusion rate of elements, and speeds up the rafting. From Table 2 and Fig. 5b it can be known that the segregation of Re makes the precipitation of TCP phase in dendrite easily. Due to no Re is consumed by TCP phase in the interdendrite, the strengthening effect of Re is obvious in the interdendrite. The diffusion rate and rafting rate are smaller, and the γ' phases are less rafted. With the influence of Re, the rafting rate in dendrite is much higher than that of interdendrite, as shown in Figs. 5 and 6. Therefore, the interdendrite is “stronger” than the dendrite [35].

4.3 The effect of TCP phase on microstructure

As shown in Fig. 4, the number of TCP phases in DD9 is higher than that of DD6, which indicates that the increase of Re content destroys the microstructure stability in some ways, mainly manifests the precipitation of TCP phase. After a long-term aging for 10 h, no TCP phase is precipitated, some of the γ' phases are connected into a stripline along the diagonal direction, and the γ phases on the strip line are truncated, as shown in the red rectangles of Fig. 5a. It can be predicted that the TCP phase will be precipitated in this stripline. After long-term aging for 15 h, many TCP phases are formed, which indicates that the temperature has an important effect on the precipitation of the TCP phase. At the high temperature, the effect of stress on the precipitation of TCP phases is decreased. The TCP phase grows along with the two perpendicular diagonal directions of the γ'

phase, which is consistent with the above predicted growth direction. It can be determined that the elements of the γ phase are consumed in the initial stage of the precipitation of the TCP phase. The γ' phases connect into a stripline and the γ phases on the strip line are truncated. At this time, no TCP phase is found. With the continuous high-temperature aging, the refractory elements such as Re continually get together along the stripline, and the TCP phase is precipitated along the stripline, as shown in Fig. 5b.

when aging for 15 h, many TCP phases are precipitated. It can be deduced that the precipitation of TCP phase is in the early stage of the long-term aging test and sensitive to the high temperature. With the increase of the aging time, the two-phase structure constantly changes. The γ' phase rafts continuously, and the γ phase is truncated. The two-phase structure near the TCP phase firstly disappears and the γ' phase near the TCP phase raft firstly, indicating that the precipitation of the TCP phase can promote the element diffusion. It can be known that the precipitation of the TCP phase greatly destroys the two-phase structure and the microstructure stability. The research shows that the TCP phase is unstable, in where cracks usually initiate and propagate [33].

4.4 Dislocation movement and element diffusion

The plastic deformation is performed by the movement of dislocations which are thought as line defects. The dislocation motion is related to the migration of atoms. There is a strong interaction between the solute atoms and dislocations. By the research on a second-generation single crystal Ni-based superalloy ERBO1, X. X. Wu et al. [36] thought that diffusion of solutes from the γ matrix into the γ' phase along the dislocation line (pipe) could explain the solute segregation at the dislocations after creep in the γ' phase. The solute atoms are often attracted to diffuse around the dislocation lines to form the Cottrell gas mass in the movement of dislocations. Therefore, the diffusion activation energy of the atom along the pipe is about 1/2 of the bulk diffusion, with a higher diffusion rate. The movement of dislocation is affected by a resistance which comes from many fields, can be written as

$$\sigma = \sigma_0 + \alpha G b \rho^{\frac{1}{2}} \tag{1}$$

where σ_0 is the P-N stress, G is the shear modulus, b is the value of the Burgers vector, ρ is the movable dislocation density, α is the material-dependent constant and usually in the range of 0.2–0.5. The expression of the crystal strain and the dislocation movement is as follows

$$\gamma = \langle m \rangle \rho b \bar{x} \tag{2}$$

The strain rate is

$$\dot{\epsilon} = \frac{d\gamma}{dt} = \langle m \rangle \rho b \frac{d\bar{x}}{dt} = \langle m \rangle \rho b \bar{v} \tag{3}$$

where γ is the shear strain, $\langle m \rangle$ is the average orientation factor, b is the value of the Burgers vector, ρ is the movable dislocation density, \bar{x} is the average movement distance of dislocations and \bar{v} is the average movement rate of dislocations. However, formula (1) doesn't consider the effect of thermal activation on stress. In fact, the temperature and strain rate have a certain influence on the resistance of the dislocation motion, so the resistance can be expressed as

$$\sigma = \sigma_T + \sigma_G \tag{4}$$

where σ_T is the part related to the temperature or the strain rate, σ_G is the part independent of the temperature or the strain rate, σ_T is the resistance resulting from the intersection of the sliding dislocation and the dislocation forest, σ_G is the elastic internal stress between dislocations. After a transformation, the resistance of dislocation motion can be written as

$$\sigma = \begin{cases} \sigma_G + \frac{U_0 - kT \ln \epsilon / \rho b d v_0}{V} & T \leq T_c \\ \sigma_G & T > T_c \end{cases} \tag{5}$$

And

$$T_c = - \frac{U_0}{k \ln \epsilon / \rho b d v_0} \tag{6}$$

where U_0 is the activation energy without the intersection of external forces, V is the activation volume, T is the temperature, d is the dislocation width and v_0 is the natural vibration frequency of the dislocation line. From formulas (5) and (6), it can be seen that the variation of shear modulus with the temperature can be ignored when the strain rate is constant [37]. The greater the strain rate is, the greater the critical temperature T_c is. When the test temperature is greater than the critical temperature, the thermal activation makes the intersection easily and no longer hinders the dislocation movement, at which time the dislocation movement only needs a small stress. The dislocations are generated in the high temperature (1100 °C) creep of the second-generation and the third-generation single crystal superalloys, as shown in Fig. 8. At this time, the dislocations mostly confined to the γ matrix channel, the dense dislocation networks are formed at the γ matrix channel and the γ/γ' interface. There are dislocations cut into the γ' phase. The possible formation of Re clusters in the γ matrix channel may hinder the dislocation motion. However, the Re clusters were neither detected by atom probe probe tomography nor by extended X-ray absorption fine structure researches [16, 38, 39]. At the γ/γ' interface, Re accumulates near dislocation cores and block their motion [40]. Meanwhile, Re segregates to the

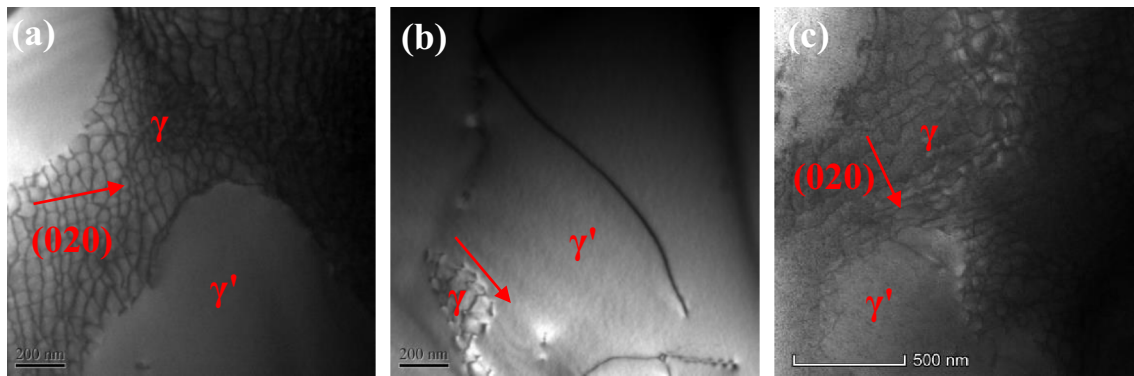


Fig. 8 The TEM BF photos of dislocations after the creep test at 1100 °C and 140 MPa: (a–b) DD6 [33], (c) DD9

dislocation inside the γ' phase. The Re content at dislocation is higher than that of the surrounding γ' phases, which is related to the pipe diffusion. In the presence of a dislocation cutting into the γ' phase and connecting the γ and the γ' phase, the solute exchange can be expected to take place along the dislocation line having a well-defined pipe cross-section [36]. Due to the larger atomic size and low diffusivity, Re segregation to dislocations blocks the motion of dislocations. Based on the above, we tend to think that the strengthening effect of Re is related to its blocking on dislocations and the pipe diffusion of Re relieve the energy caused by the blocking, the process of which is dynamic equilibrium. The researches show that the pipe diffusion is contribution to the precipitates [41, 42]. The literature [33] inferred that the enrichment of Re in the TCP phase is the result of short circuit diffusion. In the combination of literature [36] and the long-term aging test in Fig. 5, we infer that the dislocation diffusion and vacancy diffusion all contribute to the precipitation of TCP phases. The vacancy diffusion should be the main reason for the precipitation of TCP phase because of the precipitation of TCP phases in the long-term aging test without dislocations. The moving dislocations should be absorbed by the region containing TCP phase, as shown in Fig. 5a.

There are a certain number of vacancies and a certain vacancy equilibrium concentration at a certain temperature in the crystal. The higher the temperature is, the greater the vacancy concentration is. The crystal with a certain vacancy concentration at a certain temperature is stable. At a high-temperature creep, due to the increase of vacancy concentration, the elements not only diffuse along dislocations but also carry out the vacancy diffusion. The vacancy diffusivity can be written as

$$D = \alpha a^2 \nu \exp\left(\frac{\Delta S^* + \Delta S_v}{R}\right) \exp\left(-\frac{\Delta H^* + \Delta H_v}{RT}\right) \quad (7)$$

The diffusion activation energy can be given as

$$Q = \Delta H^* + \Delta H_v \quad (8)$$

where α is the geometric factor related to the crystal structure, a is the lattice constant, ν is the frequency of the atoms vibration to the vacancy, T is the temperature, ΔS^* is the activation entropy, ΔS_v is the vacancy formation entropy, ΔH^* is the activation enthalpy, and ΔH_v is the vacancy formation enthalpy [43, 44]. At the high-temperature creep, when the temperature is stable, the entropy value reaches the maximum, and the activation entropy and vacancy formation entropy decrease. Because of the high temperature, the value of $\exp\left(-\frac{\Delta H^* + \Delta H_v}{RT}\right)$ and the frequency of atoms vibration to vacancies increase. According to formulas (7) and (8), the diffusion coefficient increases and the diffusion activation energy decreases. The element Re easily carries out the vacancy diffusion at the high temperature. The migration of Re destroys the inherent structure and affects the properties of the alloy, which is directly manifested in the strengthening effect and the precipitation of TCP phases. The enrichment of Re in TCP phase of the long-term aging test is the vacancy diffusion. In general, the vacancy and the dislocation are formed at the defect site. The dislocations and the vacancies themselves are also crystal defects. Therefore, it can be inferred that where the higher the crystal defect content, where the easier to precipitate the TCP phase. The element Re can hinder the movement of dislocations and promote the precipitation of TCP phases. The movement of dislocations can promote the diffusion of Re and the precipitation of TCP phases.

5 The role of Re on the development of single-crystal superalloys

The strengthening effect of Re on single-crystal superalloys in service is obvious, and the side effect of Re on the microstructure stability can also not be ignored. It is significantly and necessary to study the effect of Re on the development

of single-crystal superalloys. In the future, we think that the development of single crystal superalloys may be able to seek breakthroughs in the following: (1) The strengthening mechanism and migration law of refractory elements such as Re in the single crystal superalloy still need to be further studied; (2) Looking for the alternative elements, such as Mo, to maintain or improve the comprehensive properties of single crystal superalloys while reducing costs; (3) The solution strengthening mechanism for material preparation need to be optimized by adjusting the Re content; (4) Adjusting the type and content of elements, such as the content of Re and Ru, to inhibit the precipitation of TCP phase, stabilize the microstructure and optimize the mechanical properties of single-crystal superalloys.

6 Conclusions

The effects of Re, dislocations, TCP phases and their interaction on creep properties and microstructure evolution were researched. The internal relations of element diffusion, dislocation movement and microstructure evolution were investigated. Some related conclusions can be drawn as follows:

- (1) The third-generation single crystal superalloys with a higher Re content have better creep properties at 1100 °C and 140 MPa than that of the second-generation single crystal superalloys. The precipitation of TCP phase is the main reason why the creep property of DD9 isn't enhanced obviously more than that of DD6.
- (2) With the higher Re content, the third-generation single crystal superalloy has a more compact and uniform two-phase structure, a lower rafting rate, and the size of the single γ' phase is smaller. The microstructure of the third-generation single crystal superalloy is more stable than that of the second-generation single crystal superalloy. The rafting rate in dendrite is much higher than that in interdendrite.
- (3) The higher the Re content, the more TCP phases are precipitated. In the initial stage of the TCP phase precipitation, the γ' phases connect into a stripline, the γ phases on the strip line are truncated, and the TCP phase is precipitated along the stripline. TCP phases can promote the diffusion of elements and accelerate the rafting of γ' phases.
- (4) High temperature can promote the movement of dislocations, form more vacancies in the crystal, increase the diffusion coefficient, reduce the diffusion activation energy, and accelerate the diffusion of Re. The element Re carries out the pipe diffusion and the vacancy diffusion at the high temperature. The TCP phase is precipitated in the region with a large number of dislocations and vacancies. The element Re can hinder the movement of dislocations and promote the precipitation of TCP phases. The movement of dislocations can promote the diffusion of Re and the precipitation of TCP phases.

Acknowledgments The research was supported by the National Natural Science Foundation of China (No. 51875461, 51875462).

References

1. R. F. Singer, *Advanced Materials and Processes for Land-Based Gas Turbines*, Materials for Advanced Power Engineering, (Kluwer Academic Publishers, Dordrecht, 1994)
2. R.C. Reed, *The Superalloys: Fundamentals and Applications* (Cambridge University Press, Cambridge, 2006)
3. T. Takaki, S. Sakane, M. Ohno, Y. Shibuta, T. Aoki, C. Gandin, *Mater.* **1**, 104 (2018)
4. M. Senge, J. Steger, A. Brückner-Foit, A. Rienäcker, *Mater.* **3**, 41 (2018)
5. H.Y. Wei, M. Xu, X.X. Liu, *J. Propul. Technol.* **2**, 60 (2012)
6. M.J. Donachie, *Superalloys: a Technical Guide* (ASM International, Materials Park, OH, 2002)
7. K. Yutaka, K. Toshiharu, Y. Tadaharu, J.X. Zhang, M. Osawa, H. Harada, Y. Aoki, M. Arai, *Warrendale* (TMS, PA, 2004), p. 35
8. S.G. Tian, J. Wu, D.L. Shu, Y. Su, H.C. Yu, B.J. Qian, *Mater. Sci. Eng. A* **616**, 260 (2014)
9. Q.Q. Ding, S.Z. Li, L.Q. Chen, X.D. Han, Z. Zhang, Q. Yu, J.X. Li, *Acta Mater.* **154**, 137 (2018)
10. P. Li, Q.Q. Li, T. Jin, Y.Z. Zhou, J.G. Li, X.F. Sun, Z.F. Zhang, *Mater. Sci. Eng. A* **603**, 84 (2014)
11. J.J. Yu, X.F. Sun, T. Jin, N.R. Zhao, H.R. Guan, Z.Q. Hu, *Mater. Sci. Eng. A* **458**, 39 (2007)
12. G.L. Erickson, *Superalloys*. **35**, 44 (1996)
13. G. Liu, L. Liu, S.X. Zhang, C.B. Yang, J. Zhang, H.Z. Fu, *Acta Metall. Sin.* **48**, 845 (2012)
14. R. Yi, H. Zhang, Y.L. Pei, S.S. Li, S.K. Gong, *Mater.* **6**, 100278 (2019)
15. P. Wollgramm, H. Buck, K. Neuking, A.B. Parsa, S. Schuwalow, J. Rogal, R. Drautz, G. Eggeler, *Mater. Sci. Eng. A* **628**, 382 (2015)
16. A. Mottura, R.T. Wu, M.W. Finnis, R.C. Reed, *Acta Mater.* **56**, 2669 (2008)
17. D.L. Shu, S.G. Tian, N. Tian, L.R. Liu, S. Liang, B.S. Zhang, *Mater. Des.* **132**, 198 (2017)
18. Z.H. Tan, X.G. Wang, L.H. Ye, G.C. Hou, R. Li, Y.H. Yang, J.L. Liu, J.D. Liu, L. Yang, B. Wang, P. Dong, J.G. Li, Y.Z. Zhou, X.F. Sun, *Mater. Sci. Eng. A* **761**, 138042 (2019)
19. B. Yin, G. Xie, L.H. Lou, J. Zhang, *Scripta Mater.* **173**, 1 (2019)
20. A. Nararak, P. Wangyao, T. Rojhirunsakool, G. Lothongkum, *Mater. Test* **61**, 609 (2019)
21. W.P. Wu, S.Y. Li, Y.L. Li, *Mech. Mater.* **132**, 9 (2019)
22. S. Tian, Y. Su, B. Qian, X. Yu, F. Liang, A. Li, *Mater. Des.* **37**, 236 (2012)
23. F.H. Latief, K. Kakehi, *Mater. Des.* **49**, 485 (2013)
24. K. Chen, L.R. Zhao, J.S. Tse, *Mater. Sci. Eng. A* **365**, 80 (2004)
25. X. Gong, G.X. Yang, Y.H. Fu, Y.Q. Xie, J. Zhuang, X. Ning, *Comput. Mater. Sci.* **47**, 320 (2009)
26. S.Y. Ma, J.X. Zhang, *Prog. Nat. Sci. Mater.* **26**, 636 (2016)
27. L.F. Zhang, Z.W. Huang, L. Jiang, J.H. Luan, Z.B. Jiao, C.T. Liu, *Mater. Sci. Eng. A* **744**, 481 (2019)
28. J. Pistor, C. Körner, *Mater. Lett. X* **1**, 100003 (2019)

29. C. Meid, M. Eggeler, P. Watermeyer, A. Kostka, T. Hamerschmidt, R. Drautz, G. Eggeler, M. Bartsch, *Acta Mater.* **168**, 343 (2019)
30. R. Popp, S. Haas, F. Scherm, A. Redermeier, E. Povoden-Karadeniz, T. Gohler, U. Glatzel, *J. Alloys. Compd.* **788**, 67 (2019)
31. H.X. Jin, J.X. Zhang, Y.J. Zhang, W.Y. Zhang, P. Li, S.Y. Ma, *Intermetallics* **113**, 106556 (2019)
32. L. Cao, P. Wollgramm, D. Bürger, A. Kostka, G. Cailletaud, G. Eggeler, *Acta Mater.* **158**, 381 (2018)
33. Z.K. Zhang, Z.F. Yue, *J. Alloys. Compd.* **746**, 84 (2018)
34. S.G. Tian, M.G. Wang, T. Li, B.J. Qian, J. Xie, *Mater. Sci. Eng. A.* **527**, 5444 (2010)
35. G. Laplanche, N. Wiczorek, F. Fox, S. Berglund, J. Pfetzinger-Micklich, K. Kishida, H. Inui, G. Eggeler, *Acta Mater.* **160**, 173 (2018)
36. X.X. Wu, S.K. Makineni, P. Kontis, G. Dehm, D. Raabe, B. Gault, G. Eggeler, *Mater.* **4**, 109 (2018)
37. D.Z. Yang, *Dislocations and Strengthening Mechanisms of Metals* (Harbin Institute of Technology Press, Harbin, 1991)
38. A. Mottura, N. Warnken, M.K. Miller, M.W. Finnis, R.C. Reed, *Acta Mater.* **58**, 931 (2010)
39. A. Mottura, M.W. Finnis, R.C. Reed, *Acta Mater.* **60**, 2866 (2012)
40. B.H. Ge, Y.S. Luo, J.R. Li, J. Zhu, *Scripta Mater.* **63**, 969 (2010)
41. S.S. Xiang, S.C. Mao, H. Wei, Y.N. Liu, J.X. Zhang, Z.J. Shen, H.B. Long, H.Y. Zhang, X.G. Wang, Z. Zhang, X.D. Han, *Acta Mater.* **116**, 343 (2016)
42. B. Dutta, E. Palmiere, C. Sellars, *Acta Mater.* **49**, 785 (2001)
43. J.S. Pan, J.M. Tong, M.B. Tian, *Fundamentals of Materials Science* (Tsinghua University Press, Beijing, 2011)
44. X. Cai, *Fundamentals of Materials Science and Engineering*, Shanghai Jiao Tong University Press, 2010.

Publisher's Note Springer Nature remains neutral with regard to jurisdictional claims in published maps and institutional affiliations.